



# Role of intra-ventricular vortex in left ventricular ejection elucidated by echo-dynamography

Motono Tanaka<sup>1</sup> · Tsuguya Sakamoto<sup>2</sup> · Yoshifumi Saijo<sup>3</sup> · Yoshiaki Katahira<sup>4</sup> · Shigeo Sugawara<sup>5</sup> · Hiroyuki Nakajima<sup>1</sup> · Takafumi Kurokawa<sup>1</sup> · Hiroshi Kanai<sup>6</sup>

Received: 27 November 2018 / Accepted: 18 March 2019 / Published online: 10 May 2019  
© The Japan Society of Ultrasonics in Medicine 2019

## Abstract

**Purpose** From the correlation between the blood flow dynamics and wall dynamics in the left ventricle (LV) analyzed using echo-dynamography, the ejection mechanisms and role of the intra-ventricular vortex in the LV were elucidated in detail during the pre-ejection transitional period (pre-ETP), the very short period preceding LV ejection.

**Methods** The study included 10 healthy volunteers. Flow structure was analyzed using echo-dynamography, and LV wall dynamics were measured using both high-frame-rate two-dimensional echocardiography and a phase difference tracking method we developed.

**Results** A large accelerated vortex occurred at the central basal area of the LV during this period. The main flow axis velocity line of the LV showed a linearly increasing pattern. The slope of the velocity pattern reflected the deformity of the flow route induced by LV contraction during the pre-ETP. The centrifugal force of the vortex at its junction with the main outflow created a stepwise increase of about 50% of the ejection velocity.

**Conclusion** Ejection of blood from the LV was accomplished by the extruding action of the ventricular wall and the centrifugal force of the accelerated vortex during this period. During ejection, accelerated outflow was considered to create a spiral flow in the aorta with help from the spherical structure of the Valsalva sinus.

**Keywords** Echo-dynamography · Vortex · Wall dynamics · Flow structure · Axial strain rate

## Introduction

As previously noted in the literature [1, 2], the blood flow from the left ventricle (LV) is an accelerated spiral flow with high velocity. Such a flow is not solely due to the pressure difference between the LV and aorta alone; therefore, the details of the ejection mechanism have yet to be elucidated. This has inspired us to clarify the detailed LV wall dynamics concomitant with the inseparable intra-ventricular blood flow structure.

However, an investigative and noninvasive methodology has not been developed to date, likely since no sufficient spatial resolution has been determined using any available technique [3–9]. Accordingly, here we aimed to examine the production mechanism of this accelerated flow and its physiological function.

By using echo-dynamography including a new analytical intra-ventricular vortex method we have developed, we attempted to elucidate the production mechanism of LV ejection and the role of the vortex in ejection according

✉ Motono Tanaka  
m.tanaka@jata-miyagi.org

<sup>1</sup> Department of Cardiovascular Medicine, Tohoku Medical and Pharmaceutical University Hospital, 1-12-1 Fukumuro, Miyagino-ku, Sendai, Miyagi 983-8512, Japan

<sup>2</sup> Hanzomon Hospital, 1-14 Kojimachi, Chiyoda-ku, Tokyo 102-0083, Japan

<sup>3</sup> Graduate School of Biomedical Engineering, Tohoku University, 4-1 Seiryomachi, Aoba-ku, Sendai, Miyagi 980-8575, Japan

<sup>4</sup> Katta General Hospital, 36 Shimoharaoki, Kuramoto, Fukuoka, Shiroishi, Miyagi 989-0231, Japan

<sup>5</sup> Nihonkai General Hospital, 30 Akiho-machi, Sakata, Yamagata 998-8501, Japan

<sup>6</sup> Department of Electronic Engineering, Tohoku University, 6-6-05 Aramaki Aza Aoba, Aoba-ku, Sendai, Miyagi 980-8579, Japan

to the correlation between the flow structure and the wall dynamics from the onset of the apical contraction to just before LV ejection, which was defined as the pre-ejection transitional period (pre-ETP) [10].

## Method and materials

### Subjects

The 10 healthy subjects aged 30–50 years ( $39.6 \pm 10.4$  years), all of whom were also included in our previous studies [10–14], provided informed consent.

### Methods

#### Measurement and analysis of blood flow structure in the LV

The ultrasonic equipment and measuring methods used in the present study were identical to those in our previous investigations [2, 10–14]. Two-dimensional (2D) echocardiographic data and 2D Doppler flow velocity data on the longitudinal cross-section of the LV passing through three points (the center of the aorta, mitral orifices, and the apex) were obtained during 10–15 cardiac cycles with quiet breathing and digitally recorded.

The Doppler flow velocity data were processed offline using our own echo-dynamography software [15–18] to obtain the flow velocity vector distribution on the observation plane, which was then overlaid onto the 2D echocardiogram [2, 10–14].

From the 2D distribution of the velocity vector, the blood flow structure appearing in the LV on the scanning plane at an arbitrary time point during the cardiac cycle, such as straight, meandering, or vortex, was qualitatively estimated [10–14]. The flow volume [19–22], velocity gradient of the flow [2, 11], and distribution of the stream line (SL) [16, 19–21] were also quantitatively estimated.

Furthermore, the following flow dynamic parameters of the vortex were obtained in the pre-ETP.

1. *Vortex diameter (VD)* determined from half the width of the maximum value of the stream function [16, 18].
2. *Circumferential velocity (CV)* obtained from the velocity vector along the circumference of the vortex [11].
3. *Velocity distribution on the SL of the vortex* estimated along the arbitrary SL.
4. *Vorticity (RT)* to differentiate the “irrotational” from the “rotational” vortex and estimate the vortex scale, the vorticity ( $\omega$ ) was calculated from the rotation of the vector on the scanning plane [22]. The positive vorticity (clockwise rotation) was shown as a cold color and the negative (counterclockwise rotation) as a warm color.

5. *Doppler pressure (DP)* [12, 17, 23] obtained from the velocity vector distribution on the scanning plane as previously reported [11, 24] and corrected by the reference pressure value at the fibrous trigone. Warm colors show positive pressure and cold colors negative pressure.
6. *Acceleration for changing the flow direction (ACFD)* [2, 11, 22] to evaluate quantitatively the vortex’s rotation power, the product of the vorticity ( $\omega$ ) and the velocity vector ( $v$ ) defined as “ACFD ( $\omega \cdot v$ )” was automatically calculated. Details can be evaluated from the profile of the vector distribution on the line passing through the center of the 2D distribution of the ACFD.

#### Analysis of LV wall thickness and dynamics

Changes in the thicknesses of the intra-ventricular septum (IVS) and posterior wall (PW) and those in the internal diameter of the LV at the apical (A: just at the papillary muscle level), basal (B: approximately 10 mm from the mitral valve ring), and central (C: in the midst of A and B) areas, as well as those of the mitral valve ring diameter (MRD) and displacement (MRM) during the cardiac cycle, were measured from 30 successive 2D echocardiograms [10–12].

#### Analysis of LV wall dynamics at the local myocardial level

On the longitudinal section plane scanned at a high speed of 630–700 frames/s, three beam directions of the basal (B), central (C) and apical (A) parts were selected by sparse scan. The echo signals of the LV wall during time intervals of 2–6 s were recorded and then processed offline using our software [24–27]. The axial strain rate (aSR) at the local myocardial tissue level was obtained using “the phase difference tracking method.” The aSR distribution was acquired by shifting the measuring point every 200  $\mu\text{m}$ . The time serial aSR distribution was overlaid in a color-coded M-mode image. A contraction was indicated by a cold color (+), while extension was indicated by a warm color (–).

## Results

Similar flow structures appeared in nearly in all cases in the pre-ETP. The results obtained in one representative case (Case 10) are shown in Figs. 1, 2, 3, and 4. Case 10 is representative because the values were in the middle range of all of the cases. Tables 1 and 2 show a summary of all cases. The findings in the early stage (ES, vortex formation stage) were compared to those in the late stage (LS, accelerated vortex stage).

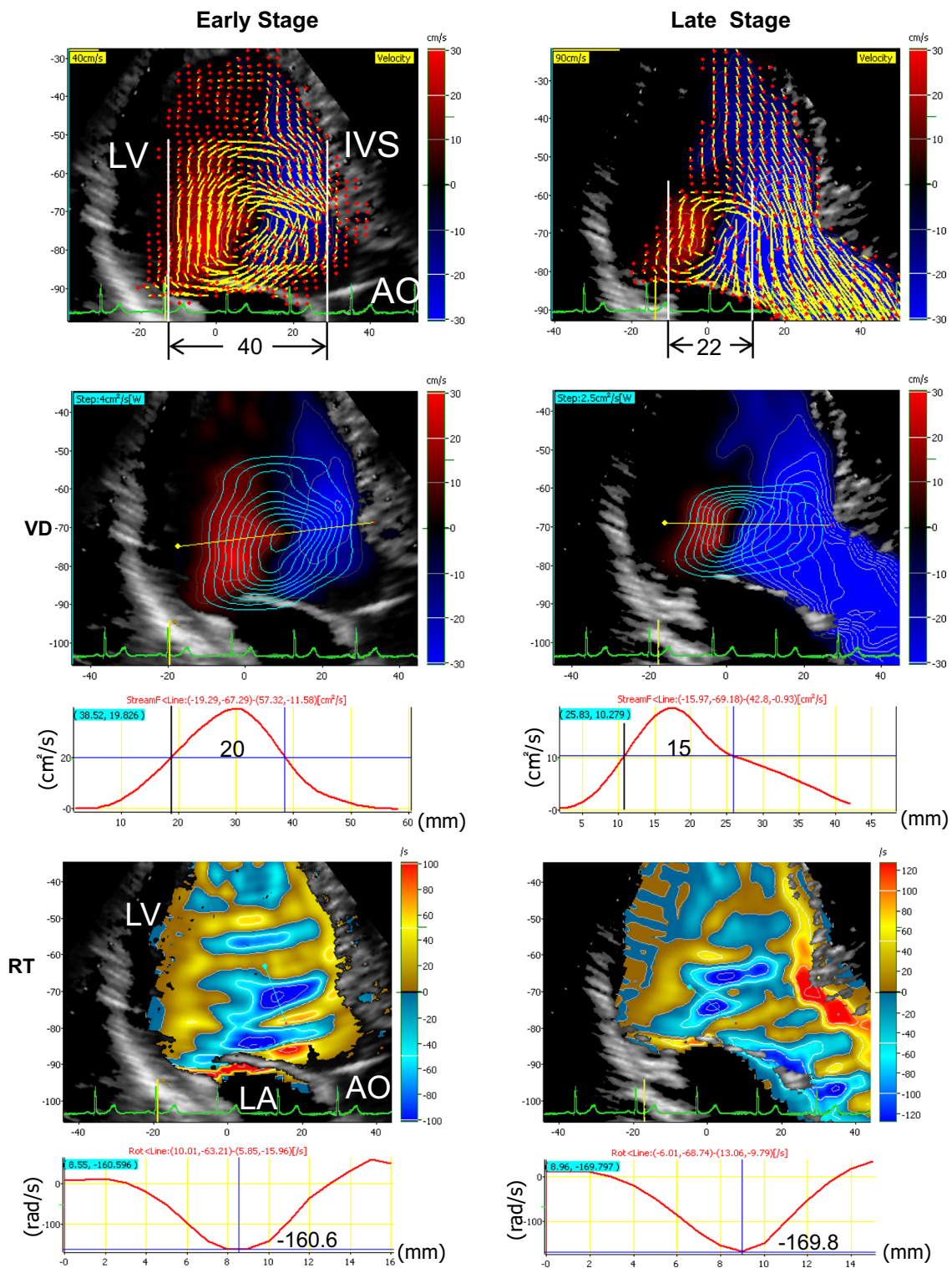


**Fig. 1** Comparison of the vortex characteristics in the left ventricle (LV) between the early stage (ES) and the late stage (LS). Left column: ES, right column: LS. Upper row: Two-dimensional distribution of the flow velocity vector on the longitudinal section plane of the LV. Middle row: Contour display of the stream function and measurement of the vortex diameter (VD). The VD was obtained from half

the width of the stream function on the yellow line. The curvilinear red graph shows the stream function distribution. Bottom row: Two-dimensional distribution of the vorticity (RT) and one-dimensional distribution of the RT on the line passing the center of the vortex. A clockwise rotation is shown as a cold color, while a counterclockwise rotation is shown as a warm color

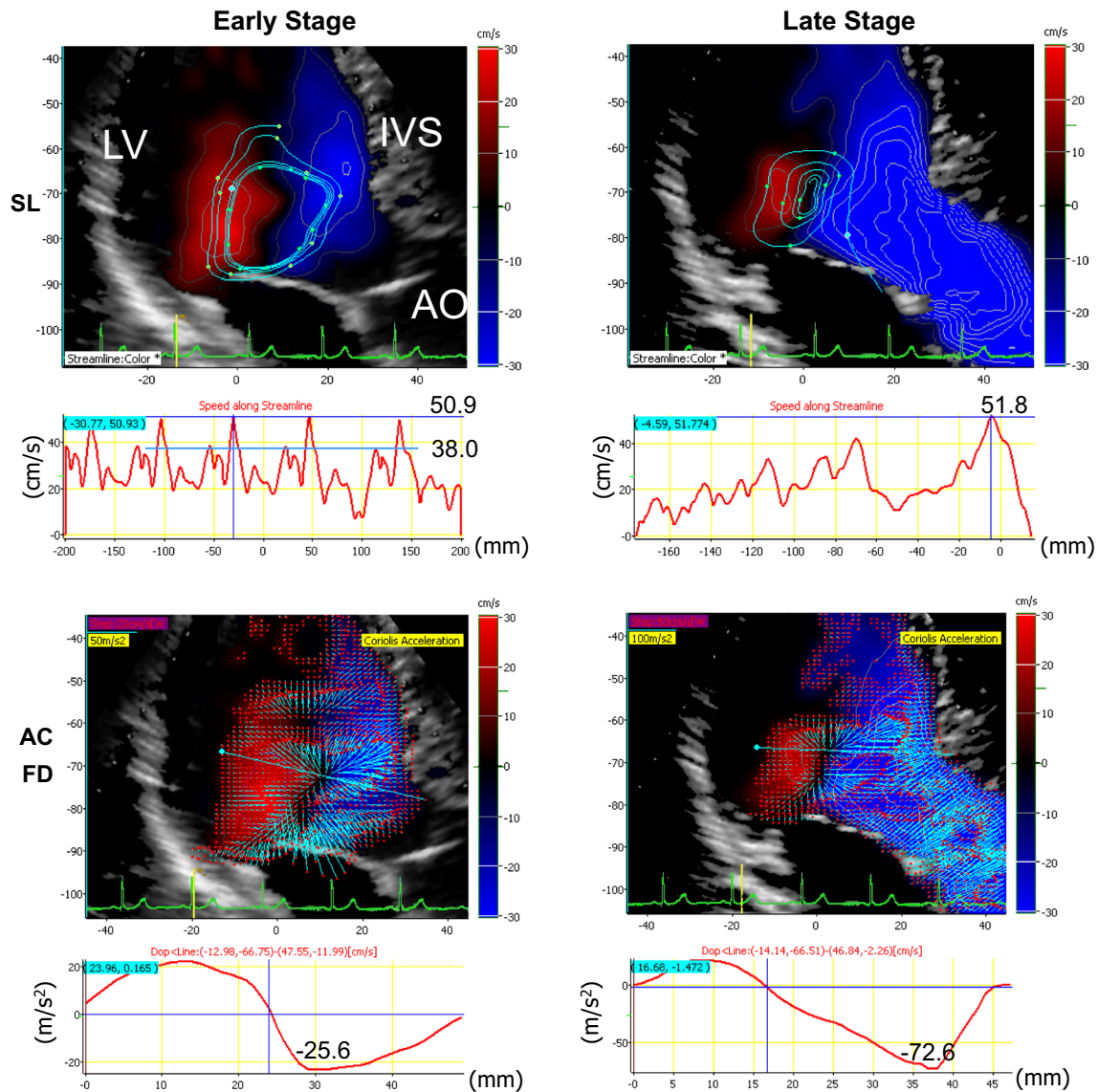


**Fig. 2** Comparison of the vortex characteristics between the early stage (ES) and the late stage (LS). Upper row: Two-dimensional distribution of the stream line (SL) on the longitudinal section plane and changes in the velocity along the SL of the vortex (curvilinear graph). The SL (blue) shows an equi-formed pattern in the ES and a spiral pattern in the LS. Bottom row: Two-dimensional distribution of the

acceleration for changing the flow direction (ACFD) of the vortex. Vector grade is shown by the length of the blue lines and direction is shown by the red mark put on the tip of the vector. A radial pattern is visible in the vortex. Reference data are shown at the upper left corner of the figure. Curvilinear graphs show the data along the blue line displayed on the two-dimensional distribution

## Flow structure in the LV appeared on the longitudinal section plane

### Velocity vector distribution of the vortex in pre-ETP

The upper row of Fig. 1 shows the velocity vector distributions of the vortex in the ES (left, 0–100 ms) and that in the LS (right, 100–220 ms) of the pre-ETP (0–220 ms).

In the vortex formation stage, the main velocity vector gradually increased and became widely distributed along the IVS from the apical posterior area to the basal area. The

velocity was about 30 cm/s in the central area, while the greatest velocity (about 51 cm/s) was seen in the basal area. Thereafter, these vectors were directed backward in the area under the aortic valve (AV). After passing under the mitral valve, the vectors were directed downward and decelerated to about 38 cm/s. The vectors were then directed forward to the IVS at the papillary muscle level showing the double structure and joined with the upward vector group. Thus a large clockwise rotational flow (vortex) with uneven velocity distribution developed. The vortex's diameter was about 40 mm.

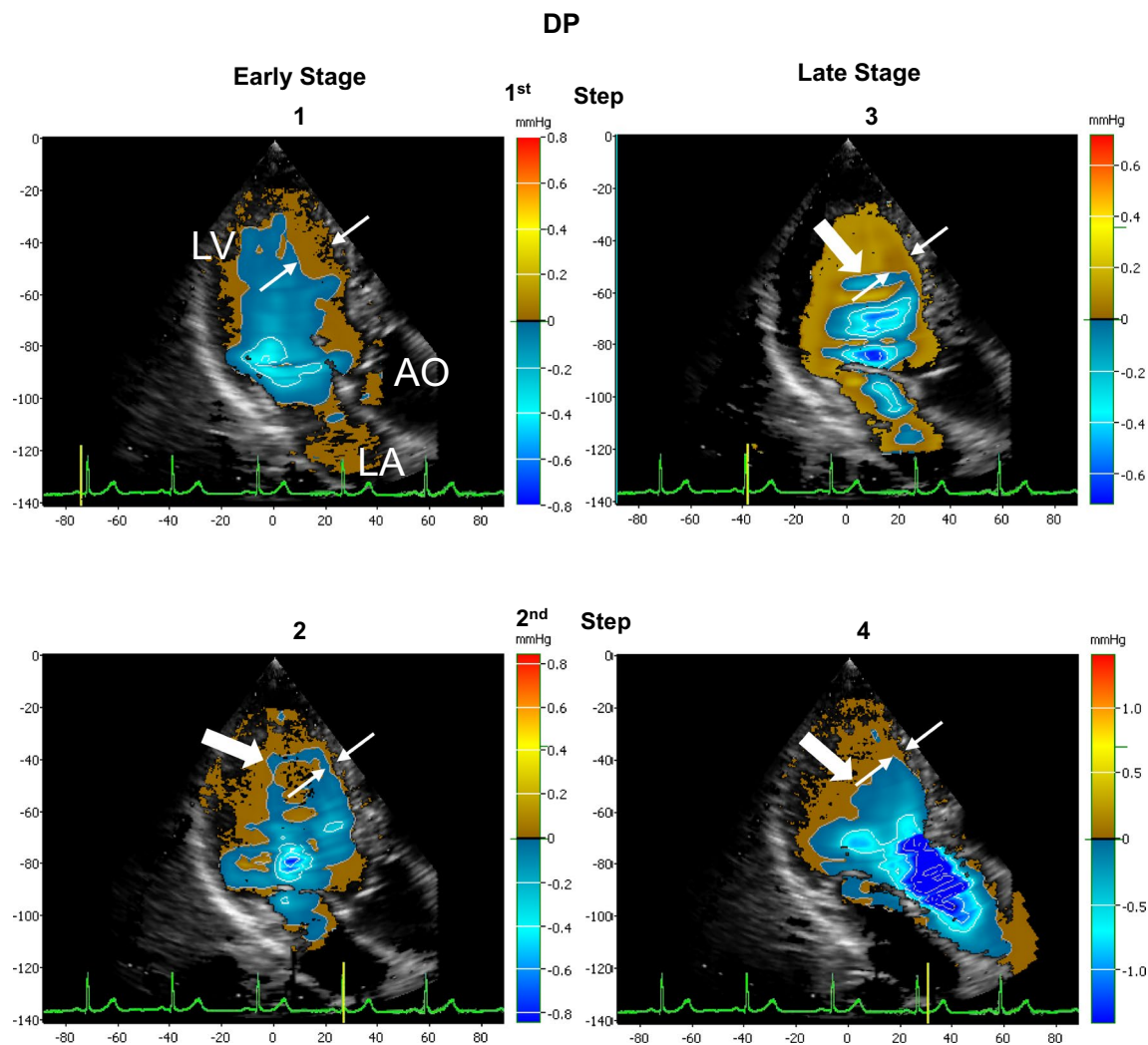


**Fig. 3** Doppler pressure distributions in the longitudinal section plane of the LV during the pre-ejection transitional period (pre-ETP) displayed on the contour line. The warm color shows positive pressure, while the cold color shows negative pressure. The pressure level is shown on the color bar on the right. The timing of the pres-

sure images is indicated by the yellow bar on the ECG. The white narrow arrows show the changes in the width of the positive pressure area during the pre-ETP. The large thick arrows show the supposed transmitting direction of the positive pressure. *LV* left ventricle, *LA* left atrium, *AO* aorta

In the accelerated vortex stage, the velocity vector in the outflow tract increased rapidly from the apical to the basal area along the IVS. The maximal velocity area shifted antero-upward at the basal area. The vortex in this stage was accelerated and its diameter decreased to about 22 mm (Fig. 1, right upper row). At the outflow tract area just under the aortic valve, one part of the vector distribution was directed to the aorta, while the other was directed posteriorly. After passing under the anterior mitral leaflet, the flow was directed downward and rotated anteriorly. Thereafter, it joined the upward flow components in the outflow tract area, producing the accelerated vortex.

As shown in the middle row of Fig. 1, the vortex diameter (VD) calculated from the stream function was about 20 mm in the ES and about 15 mm in the LS, consequently

decreasing by about 25% in LS; the double structure disappeared. The RT was about 160.6 rad/s in the ES and about 169.8 rad/s in the LS, and a slight increase in RT appeared.

The maximum rotating velocity on the SL increased from about 50.9 cm/s in the ES to about 51.8 cm/s in the LS (Fig. 2, upper row). The rotation mode of the vortex displayed by the SL showed a repetitive circular pattern in the ES, whereas the revolution velocity increased in the outer compared to the inner part of the vortex and the accelerated vortex (spiral pattern) was observed in the LS. Since the magnitude of the ACFD vector was about  $25.6 \text{ m/s}^2$  in the ES and about  $72.6 \text{ m/s}^2$  in the LS (Fig. 2, lower row), the ACFD in the LS was remarkably increased to about 2.8 times larger than that in the ES.

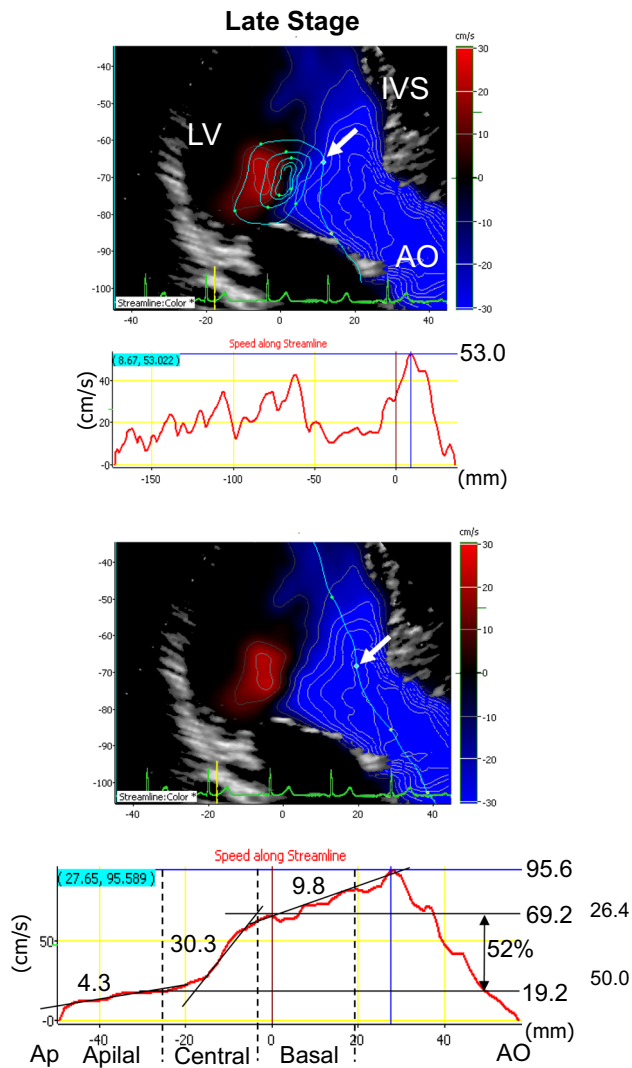


**Fig. 4** Effect of the accelerated vortex on the main outflow in the late stage (LS). Upper row of the figure and red graph: The stream line (SL) of the vortex and flow velocity distribution along the stream line of the vortex. Lower row of the figure and red graph: The SL of the main outflow and flow velocity distribution along the SL. White arrows: Positions of the 0 point in the distance scale on the curvilinear red graph (one dimensional velocity distribution) and rough junction area of the vortex and main outflow. *AO* aorta, *Ap* apex

Observing the changes in parameters of the vortex (Table 3) during the LS with the time duration of 120 ms, the number of revolutions (Rev) increased about three times, while centrifugal force (CRF) increased about two times. These results indicated that the vortex in the LS was accelerated despite the diameter decreasing.

### Doppler pressure distribution during pre-ETP

As shown in Fig. 3, the negative pressure area (blue) at the center of the vortex decreased from about  $-0.57$  mmHg to

$-0.8$  mmHg and shifted from the area just under the mitral leaflets (Fig. 3b) to the antero-upward area of the outflow tract (Fig. 3c). Moreover, the distribution pattern of the negative pressure changed from a double circular pattern in the central area (Fig. 3c) to a widely diffuse pattern in the outflow area (Fig. 3d).

The positive pressure was widely distributed in the area contacting the inner surface of the PW and IVS. The positive pressure area (brown), as shown by the thick white arrow, gradually shifted upward from the apical area to the area under the aortic valve together with a slight increase in the positive pressure ( $0.1$ – $0.2$  mmHg). Also, as shown by the white thin arrows in Fig. 3a–d, the width of the positive pressure area near the IVS changed reciprocally from wide to narrow during the pre-ETP.

These results indicated that the changes in the pressure distribution of the vortex yielded by the non-uniform distribution of the rotation speed, which knocked the IVS reciprocally, produced the mechanical oscillation of the IVS.

### Effect of the vortex on outflow blood

The effect of the vortex on the LV outflow was estimated from changes in the velocity distribution along the SL of the main outflow. As shown in Fig. 4, the velocity in the main outflow was abruptly increased from about  $19.2$  cm/s to about  $69.2$  cm/s by about 52% of the maximal ejection velocity ( $95.6$  cm/s) at the confluent area (white arrow) of the vortex and the main outflow. The step-up increase in velocity was about 30.3 in the velocity gradient.

Consequently, the blood flow velocity of about  $19.2$  cm/s in the apical area was accelerated to about  $95.6$  cm/s in the basal area. These results indicated that the accelerated vortex in the late stage during pre-ETP was very useful for LV ejection and contributed greatly to the accelerated outflow in the early ejection phase.

### Wall dynamics measurement

#### Wall dynamics measured by 2D echocardiography

Figure 5 summarizes the results obtained from the 10 cases. In the early stage (ES), the apical (A, green) and central (C, yellow) parts were in a contracting state that began at the P of ECG; nevertheless, the basal part (B, blue) began to extend slightly, as shown in the change in thickness of the posterior wall (PWT) of the unshaded area in the upper row of Fig. 5. The thickness change in the IVS was very small compared with that in the posterior wall [10, 13].

In the late stage (LS), thickness of the apical part was increased, whereas the central and basal parts extended under a contracting state. Although the internal diameter of the LV (LVD) showed temporal dilatation during atrial

**Table 1** Measurement data of the vortex appeared in the basal area of the LV in the early and late stages of pre-ETP in 10 normal cases

Case no.	SEX	Age	EF (%)	ES			LS			
				LVDd (mm)	VD (mm)	VD/LVDd	Vmax (cm/s)	OV (cm/s)	Vmax/OV (%)	VF (cm <sup>2</sup> /s)
1	F	49	66	46	20.8	0.45	37.2	95.1	39.1	36.7
2	F	33	59	42	22.2	0.53	31.8	93	34	32.6
3	M	32	60	46	19.3	0.42	66.8	85.7	78	43.2
4	M	43	61	54	20.3	0.38	37.6	94.5	40	38.9
5	M	31	60	45	20.5	0.46	52.2	71.5	73	31.6
6	M	34	68	49	22.2	0.45	48.7	94.5	51	30
7	F	37	61	48	19.9	0.41	35.9	108.5	33	28.1
8	F	43	67	53	19.2	0.36	32.5	76.5	42	41.2
9	F	50	55	48	23.1	0.48	34.7	99.6	35	32.9
10	F	44	55	50	20	0.40	44.1	95.6	46	53.7
Ave		39.6	61.2	48.1	20.8	0.43	42.2	91.5	47.1	36.9

EF ejection fraction, LVDd end-diastolic left ventricular diameter, VD diameter of the vortex, Vmax maximum velocity of the vector, OV outflow velocity, and VF flux of the vortex

**Table 2** Comparison of the characteristics of the vortex in the early stage (ES) and that in the late stage (LS) of the pre-ETP in 10 cases

Case no.	Early Stage (Pre-ETP)			Late Stage (Pre-ETP)		
	RT (rad/s)	DP (mmHg)	ACFD (m/s <sup>2</sup> )	RT (rad/s)	DP (mmHg)	ACFD (m/s <sup>2</sup> )
1	- 131.0	- 0.95	29.3	- 137.7	- 0.24	82.8
2	- 90.9	- 0.63	22.6	- 59.4	- 1.01	56.9
3	- 251.1	- 1.40	21.0	- 158.1	- 0.34	42.0
4	- 101.8	- 0.41	23.4	- 106.7	- 0.47	43.1
5	- 100.4	- 0.65	26.0	- 80.4	- 0.37	38.6
6	- 88.5	- 0.27	24.2	- 101.8	- 0.26	93.1
7	- 141.0	- 0.70	15.7	- 101.4	- 0.11	93.9
8	- 108.0	- 0.44	30.6	- 120.3	- 0.46	97.8
9	- 100.8	- 0.86	22.3	- 104.1	- 0.22	85.5
10	- 160.6	- 0.57	25.6	- 169.8	- 0.67	72.6
Average	- 127.4	- 0.69	24.1	- 114.0	- 0.42	70.6
SD	49.35	0.32	4.23	33.71	0.26	23.45

RT vorticity (-, clockwise rotation), DP Doppler pressure, and ACFD acceleration for changing the flow direction

**Table 3** Changes in characteristics of the vortex accompanied by changes in the diameter of the vortex during the late stage

VD (mm)	Circ. (mm)	Vmax (cm/s)	TD (msec)	Distance (mm)	Rev	CFR
20	62.8	52	ES: 100	51.0	0.8	1.0
15	47.1	52	LS: 120	62.4	1.3	1.4
10	31.4	42	LS: 120	50.4	1.6	1.4
5	15.7	35	LS: 120	42.0	2.7	1.9

VD vortex diameter, Circ circumference, Vmax maximum velocity, Distance revolutionary distance (distance/Circ), TD time duration, ES early stage of pre-ETP, LS late stage of pre-ETP, Rev the number of revolutions of the vortex under the assumption that the duration of the TD was 100 ms in ES and 120 ms in LS, CFR ratio to the centrifugal force of the vortex

contraction, it was almost unchanged at the apical part (A, black) and increased at the basal part (B, red) during pre-ETP. These results show the coexistence of wall contraction and extension in this period.

**Wall dynamics measured at the local myocardial level**

As shown in the middle of Fig. 5, throughout the ES, in the

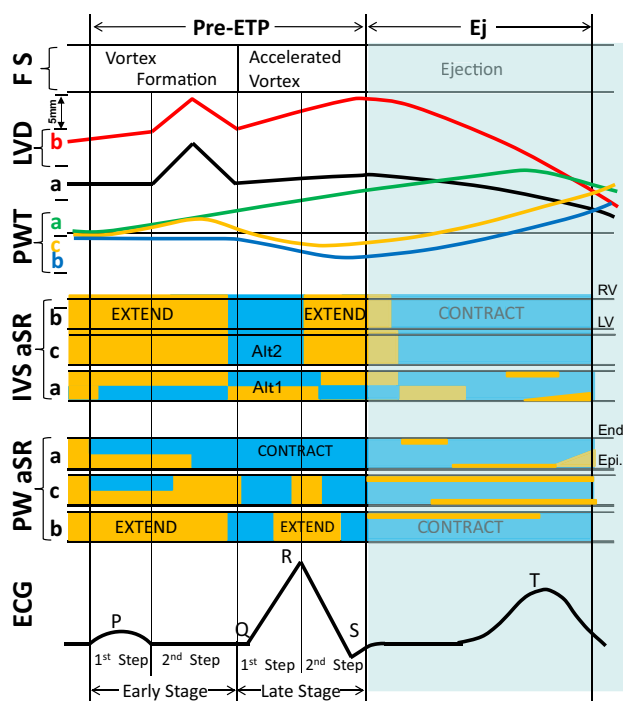


**Fig. 5** Schematic representation of the correlation among left ventricular wall dynamics, axial strain rate (aSR) distribution, and flow structure (FS) during the pre-ETP (unshaded area) and the ejection period (Ej). Curvilinear graph: Changes in thickness of the posterior wall (PWT) and that of the internal diameter of the LV (LVD) at the apical (a, green or black line), basal (b, blue or red line), and central (c, yellow line) parts. Color bar graph: Changes in timing and duration of myocardial contraction (blue color) and extension (yellow color) observed in the apical (a), central (c), and basal (b) parts in the IVS (IVS aSR) and PW (PW aSR). *Pre-ETP* pre-ejection transitional phase, *Ej* ejection, *FS* flow structure, *LVD* left ventricular diameter, *PWT* posterior wall thickness, *IVS aSR* interventricular septum aSR distribution, *PW aSR* posterior wall aSR distribution, *Alt1* bending oscillation, *Alt2* thickness oscillation, *ECG* electrocardiogram, *End* endocardium, *Ep* epicardium, *RV* right ventricle, *LV* left ventricle

apical part (A) of the PW (PW aSR) and IVS (IVS aSR), both the extension ((-)SR, orange) in the epicardial side and the contraction ((+)SR, blue) in the endocardial side began at the P wave of the ECG. In the basal part (B), the extension ((-)SR) from the endocardial to epicardial side was seen in the PW and IVS.

In the LS, the apical part (A) of the PW was in the contracting state ((+)SR). At the basal (B) and central (C) parts of the PW, after the temporal contraction ((+)SR), the extension ((-)SR) appeared, followed by the contraction ((+)SR). These changes indicated that the thickness vibration appeared in the PW.

In the IVS, alternating distribution 1 (bending oscillation), in which contraction ((+)SR) and extension ((-)SR) appeared reciprocally in the endocardium and epicardium, was seen at the apical part. On the other hand, alternating distribution 2 (thickening oscillation), in which contraction

((+)SR) and extension ((-)SR) appeared repeatedly in the myocardium, was seen at the central and basal parts of the IVS [13].

## Discussion

To elucidate the ejection mechanism, it is necessary to simultaneously measure LV wall dynamics during the cardiac cycle and accompanied flow structure dynamics together with the hemodynamics. Changes in both the LV wall and the flow dynamics can be easily estimated from the velocity information obtained by the echo methods. In the present study, the ejection mechanism was elucidated noninvasively using echo-dynamography in addition to the detailed analytical method of the vortex in the LV. Understanding of the ejection mechanism may lead to very early prediction of heart failure.

### Contribution of LV wall dynamics to ejection

The dynamic change of the LV wall during the pre-ETP is considered to appear as the ejected blood flow occurs along the main outflow axis line of the LV, which is connected by the apex to the center of the aortic valve ring [11, 14]. The maximum flow velocity distribution along the outflow axis line in the late stage is shown in the bottom row of Fig. 4.

As shown in the upper row of Fig. 5 and in the apical area (Fig. 6a), change in the wall thickness was large, but that in the internal diameter of the ventricle was small during the pre-ETP. In the basal area (Fig. 6b), the internal space of the ventricle dilated, but change in the wall thickness was small, whereas the outflow tract area was funnel-shaped and wide in the central area and narrow in the area just under the aortic valve. Changes in the velocity distribution along the main flow axis line caused by LV wall deformation will be reflected in the changes in the flow route shape, especially in route width.

As a result, the maximum blood flow velocity in the LV during pre-ETP will be shown as a linearly increasing pattern for which the gradient will be small in the apical area and large in the basal area. As shown in the bottom row of Fig. 4, the distribution showed a linearly increasing pattern with a gradient of about 9.8 and about 26.4 cm/s in velocity at the basal area, and a gradient of about 4.3 and about 19.2 cm/s in velocity at the apical area. These results were thought to reflect the changes of the flow route shape caused by deformation of LV contraction during the pre-ETP.

However, at the central area, a rapidly increasing curve with a gradient of about 30.3 and about 50.0 cm/s in increment velocity was seen despite the wide flow route. These increments are thought to be caused by another energy supply other than transformation of the flow route. After

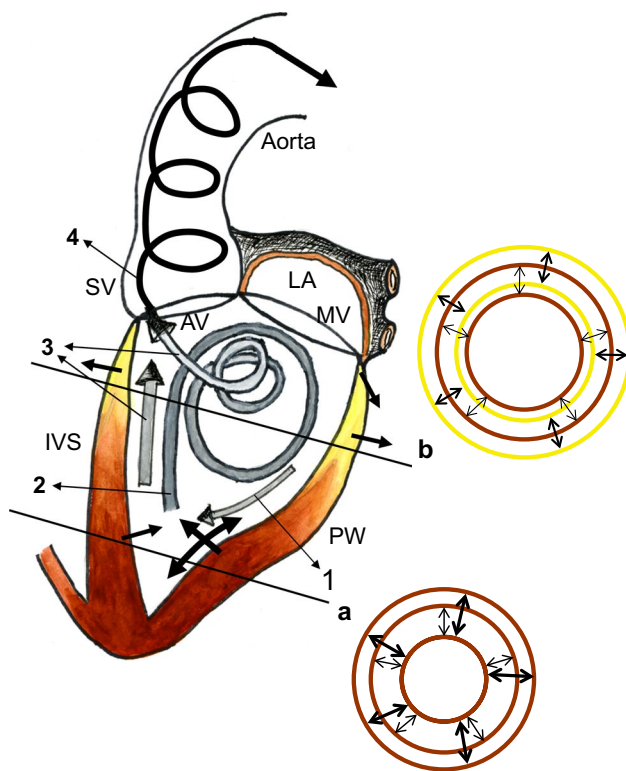


**Fig. 6** Schematic representation of the correlation between the flow structure of the vortex in the left ventricle (LV) displayed by the presumptive path line and wall dynamics of the LV appearing during the pre-ETP. Brown area: contracting part of the wall, Yellow area: extending part. Thick black arrows in the wall: moving direction and grade, Thick gray arrows: path line of the intra-ventricular flow during pre-ETP, 1: residual flow due to the atrial contraction (AC), 2: large rotating flow during the ES, 3: accelerated rotating flow during the LS and main flow from the apical area, 4: the spiral flow in the aorta, Upper right figure (b): schematic representation of the LV wall deformation appearing on the short axis cross-section at the basal part during the LS, Lower right figure (a): that at the apical part during the LS. LA left atrium, MV mitral valve, AV aortic valve, IVS inter-ventricular septum, SV sinus Valsalva, PW posterior wall

observing the blood flow structure, we suspect that this rapid increase in the velocity was caused by the kinetic energy of the vortex in the central area.

### Contribution of the vortex in the ventricle to ejection

As shown in LVD and PWT of Figs. 5 and 6a, under the LV wall dynamics in the early stage of the pre-ETP, the pressure gradient appeared to flow from the apical area of the LV wall to the IVS, as shown by the white thick arrows in Fig. 3. The positive pressure (brown in Fig. 3) was transmitted from the apical area to the basal area. At this time, as shown by the brown and yellow circles in Fig. 6b, the internal diameter increased, but the wall thickness increased little or decreased in spite of the contracting state. Thus, the

large vortex appeared at the central and basal areas in the early stage (Fig. 1, left upper row).

In the subsequent LS, the apical part and the papillary muscles gradually extruded antero-upward into the ventricle with thickness (thick black arrows at the apical part of Fig. 6). Not only was the center of the vortex displaced from just under the anterior mitral leaflet to the outflow area but also the vortex was spherical, the double structure had disappeared, and the diameter was remarkably diminished (Fig. 1, right upper row). Both the rotating velocity and the number of revolutions of the vortex increased by about two times higher than those in the ES. The ACFD increased about three times higher than that in the ES (Tables 1, 2), and that was in almost total agreement with the changes in velocity distribution (about 50.0 cm/s) shown in the lowest row of Fig. 4. The rotation velocity increased further outside than inside the vortex. Thus, the vortex accelerated with a large centrifugal force. When this accelerated vortex joined the blood flow in the outflow tract, the outflow blood velocity was increased from 19.2 to 69.2 cm/s [about 52% of the ejected velocity (95.6 cm/s)] by the centrifugal force of the accelerated vortex. These facts suggest that the accelerated vortex in the pre-ETP produces almost half of the ejection velocity and plays an important role in the LV ejecting function.

### Contribution of the accelerated vortex to cardiac function

1. The maximum velocity area of the main outflow was made to shift in the antero-upward direction just under the aortic orifice by the accelerated vortex. At the beginning of the ejection, the spiral ejecting flow was produced in the aorta by aid of the spherical shape of the Valsalva sinus (Figs. 4, 5, 6).
2. The accelerated vortex caused equalization of the intra-ventricular pressure just under the mitral leaflet and contributed to pushing up and evenly straining the mitral valve leaflets from the ventricular side (Fig. 4). Accordingly, the valve leaflets closely contacted each other and uniform tension appeared.
3. The velocity vector distribution pattern near the IVS showed a wave pattern, as seen in the ES in Fig. 1. Additionally, as shown in Fig. 3, the width of the positive pressure area near the IVS (interval between the two white thin arrows in Fig. 3) was reciprocally wide and narrow. These results indicated that the power produced by the predominant contraction of the myocardium in the PW was given to the IVS via the vortex within the ventricle. Thus, the thickness changed such that oscillation in the IVS occurred and the alternated distribution 1 (bending oscillation) and alternated distribution 2 of aSR (thickening oscillation) appeared in the septum

(IVS aSR) [13]. These changes in IVS thickness indicate the genesis of the low-frequency components of the first heart sound [28, 29].

## Limitations

The present study had several limitations. First, the number of cases was rather small, precluding a statistical analysis. Second, the technology used here was developed in our laboratory and is not currently accessible by other investigators. Finally, we must validate the clinical feasibility by investigating cases of various pathological conditions. Therefore, further observations are essential.

## Conclusions

- 1 The vortex with a double structure and uneven velocity distribution appeared at the central to basal areas of the LV in the ES of the pre-ETP. This vortex transformed to an accelerated one at the basal area in the LS.
- 2 Ejection of blood from the LV was accomplished by a combination of the following two mechanisms:
  1. Extruding action of the ventricular wall produced by narrowing of the LV chamber due to myocardial contraction.
  2. The centrifugal force of the accelerated vortex developed by spatial deformation of the LV structures.

These two mechanisms contributed at nearly similar rates (50%) at the same time.

3. This accelerated vortex acted as a promoter of the spiral flow in the aorta and oscillated the IVS. This oscillation is thought to participate in the genesis of the first heart sound.
4. From a clinical and pathophysiological point of view, the accelerated vortex in the pre-ETP played a very important role in the pump function, especially for the effective blood ejection from the LV.

## Compliance with ethical standards

**Conflict of interest** There are no financial or other relations that could lead to a conflict of interest.

**Ethical approval** All procedures followed were in accordance with the standards of the Ethics Committee for Human Research (institutional and national) and with the Helsinki Declaration of 1975, as revised in 2008.

## References

1. Kilner PJ, Yang GZ, Mohiaddin RH, et al. Helical and retrograde secondary flow pattern in the aortic arch studied by three-directional magnetic resonance velocity mapping. *Circulation*. 1993;88:2235–47.
2. Tanaka M, Sakamoto T, Sugawara S, et al. Spiral systolic blood flow in the ascending aorta and aortic arch analyzed by echodynamography. *J Cardiol*. 2010;56:97–110.
3. Braunwald E, Sonnenblick EH, Ross J Jr. Contraction of the normal heart. In: Braunwald E, editor. *Heart disease*. 2nd ed. Philadelphia: WB Saunders Co.; 1984. p. 409–46.
4. Rushmer RF. Functional anatomy and control of the heart. In: Rushmer RF, editor. *Cardiovascular dynamics*. 4th ed. Philadelphia: WB Saunders Co.; 1976. p. 76–131.
5. Ishida N, Takishima T (1992) *Cardiodynamics and its clinical application*. In: Ishida N, Takishima T (eds) 2nd ed. Bunkodo Co., Tokyo. p 1–214.
6. Arheden H, Stahlberg F (2013) Blood flow measurement. MRI and CT of the cardiovascular system. In: Higgins CB, Roos A., Lippincott, et al. (eds) 3rd edn. Philadelphia. p 75–92.
7. Tanaka M, Miyatake K, Kanbe T, et al. (1988) Application of the ultrasonic Doppler method. In: Jpn. Soci. Ultras. Med. (eds) *Diagnostic Ultrasound, principles and clinical applications*. Igaku-Shoin Ltd., Tokyo. p 167–230.
8. Tanaka M. Usefulness of ultrasonic imaging in the medical field. In: Shimizu H, Chubachi N, Kushibiki J, editors. *Acoustical imaging*. New York: Plenum Press; 1989. p. 453–66.
9. Tanaka M (1998) Historical perspective of the development of echocardiography and medical ultrasound. In: Schneider SC, Levy M, McAvoy BR (eds) *Proceedings of IEEE ultrasonics symposium*. IEEE Inc, New York. p. 1517–24.
10. Tanaka M, Sakamoto T, Sugawara S, et al. A new concept of the contraction-extension property of the left ventricular myocardium. *J Cardiol*. 2014;63:313–9.
11. Tanaka M, Sakamoto T, Sugawara S, et al. Blood flow structure and dynamics, and ejection mechanism in the left ventricle: analyzing using echo-dynamography. *J Cardiol*. 2008;52:86–101.
12. Tanaka M, Sakamoto T, Sugawara S, et al. Physiological basis and clinical significance of left ventricular suction using echodynamography. *J Cardiol*. 2011;58:232–44.
13. Tanaka M, Sakamoto T, Katahira Y, et al. Non-uniform distribution of the contraction/extension (C-E) in the left ventricular myocardium related to the myocardial function. *J Cardiol*. 2014;64:401–8.
14. Tanaka M, Sakamoto T, Sugawara S, et al. Deformability of the pulsating left ventricular wall: a new aspect elucidated by high resolution ultrasonic methods. *J Cardiol*. 2017;69:462–70.
15. Ohtsuki S, Tanaka M, Okujima M. A method of flow vector mapping deduced Doppler data on scanned plane. In: Shimizu H, Chubachi N, Kushibiki J, editors. *Acoustic imaging*. New York: Plenum Press; 1989. p. 467–72.
16. Ohtsuki S, Tanaka M. Flow function for streamlines representative of the flow on a plane in three-dimensional flow. *J Visual Soc Jap*. 1998;18:136–40.
17. Ohtsuki S, Tanaka M. Doppler pressure field deduced from the Doppler velocity field in an observation plane in a fluid. *Ultrasound Med Biol*. 2003;29:1431–8.
18. Ohtsuki S, Tanaka M. The flow velocity distribution from the Doppler information on a plane in three dimensional flow. *J Vis*. 2006;9:69–82.
19. Tanaka M, Nitta S, Yamamoto A, et al. Development and application of non-invasive method for the evaluation of cardiac function, Quantifying intracardiac blood flow. *Asian Med J*. 1994;37:283–6.

20. Tanaka M, Nitta S, Yamamoto A, et al. Development and application of non-invasive methods for the evaluation of cardiac function: measuring cardiac function. *Asian Med J.* 1994;37:397–400.
21. Tanaka M, Yamamoto A, Endo N, et al. (1992) Evaluation of the behavior of blood flow in heart chambers by means of stream line distribution method. In: Visualization Soc Jap editor. *Atlas of visualization.* Pergamon Press, Oxford. p. 205–219.
22. Hino M. Introduction to fluid mechanics. In: Hino M, editor. *Fluid dynamics.* Tokyo: Asakura Book Co.; 2002. p. 28–362.
23. Tanaka M, Nitta S, Yamamoto A, et al. Development and application of non-invasive method for the evaluation of cardiac function, Visualization of pressure changes in heart chambers. *Asian Med J.* 1994;37:341–4.
24. Yoshiara H, Hasegawa H, Kanai H, et al. Ultrasonic imaging of propagation of contraction and relaxation in heart walls at high temporal resolution. *Jpn J Appl Phys.* 2007;46:4889–96.
25. Tanaka M, Kanai H, Sato M, et al. Measurement of the moving speed of local myocardial tissue by using the phase difference tracking method and its clinical significance. *J Cardiol.* 1996;28:163.
26. Kanai H, Hasegawa H, Chubachi N, et al. Noninvasive evaluation of local myocardial thickening and its color-coded imaging. *IEEE Trans Ultrason Ferroelect Freq Contr.* 1997;44:752–68.
27. Kanai H, Hasegawa H, Chubachi N, et al. Non-invasive evaluation of spatial distribution of local instantaneous strain energy in heart wall. In: Lees S, Ferrari LA, editors. *Acoustic imaging.* New York: Plenum Press; 1997. p. 187–92.
28. Tanaka M. *Ultrasonic diagnosis of the heart.* Tokyo: Medical Electro Times Ltd; 1978. p. 118–28.
29. Ueda H, Kaito G, Sakamoto T. *Clinical Phonocardiography-Auscultation of the Heart and Phonocardiography.* Tokyo: Medical Electro Times Ltd; 1978. p. s100–s239.

**Publisher's Note** Springer Nature remains neutral with regard to jurisdictional claims in published maps and institutional affiliations.